

1 **Modeled variations of the inherent optical properties of summer
2 Arctic ice and their effects on the radiation budget: A case based on
3 ice cores from CHINARE 2008–2016**

4 Miao Yu¹, Peng Lu^{1*}, Matti Leppäranta², Bin Cheng³, Ruibo Lei⁴, Bingrui Li⁴, Qingkai Wang¹, Zhijun Li^{1*}

5 ¹State Key Laboratory of Coastal and Offshore Engineering, Dalian University of Technology, Dalian, China

6 ²Institute of Atmosphere and Earth Sciences, University of Helsinki, Helsinki, Finland

7 ³Finnish Meteorological Institute, Helsinki, Finland

8 ⁴MNR Key Laboratory for Polar Science, Polar Research Institute of China, Shanghai, China

9 *Corresponding to:* Peng Lu (lupeng@dlut.edu.cn), Zhijun Li (lizhijun@dlut.edu.cn).

10 **Abstract.** Variations in Arctic sea ice are not only apparent in its extent and thickness but also in its internal properties under
11 global warming. The microstructure of summer Arctic sea ice changes due to varying external forces, ice age, and extended
12 melting seasons, which affect its optical properties. Sea ice cores sampled in the Pacific sector of the Arctic obtained by the
13 Chinese National Arctic Research Expeditions (CHINARE) during the summers of 2008 to 2016 were used to estimate the
14 variations in the microstructures and inherent optical properties (IOPs) of ice and determine the radiation budget of sea ice
15 based on a radiative transfer model. The variations in the volume fraction of gas bubbles (V_a) of the ice top layer were not
16 significant and V_a of the ice interior layer was significant. Compared with 2008, the mean V_a of interior ice in 2016 decreased
17 by 9.1%. Meanwhile, the volume fraction of brine pockets increased clearly during 2008–2016. The changing microstructure
18 resulted in the scattering coefficient of the interior ice decreasing by 38.4% from 2008 to 2016, while no clear variations can
19 be seen in the scattering coefficient of the ice top layer. These estimated ice IOPs fell within the range of other observations.
20 Furthermore, we found that variations in interior ice were significantly related to the interannual changes in ice ages. At the
21 Arctic basin scale, the changing IOPs of interior ice greatly changed the amount of solar radiation transmitted to the upper
22 ocean even when a constant ice thickness is assumed, especially the thin ice in marginal zones, implying the presence of
23 different sea ice bottom melt processes. These findings revealed the important role of the changing microstructure and IOPs
24 of ice in affecting the radiation transfer of Arctic sea ice.

25 **1 Introduction**

26 The recent rise in air temperature in the Arctic is almost twice the global average, known as Arctic amplification (Dai et
27 al., 2019), which has been seen in the retreat of sea ice, especially in summer. The extent of sea ice in summer has decreased
28 (Comiso et al., 2008; Parkinson & Comiso, 2013; Petty et al., 2018), and summer ice is thinner (Kwok, 2018), younger (Stroeve
29 and Notz, 2018), and warmer (Wang et al., 2020) than before. These changes have affected the transfer of sunlight into the

30 Arctic Ocean, and the optical properties of sea ice are changing the solar radiation budget in the area.

31 Variations of Arctic sea-ice cover are related not only to the macroscale properties described above but also to the ice
32 microstructure. Sea ice is a multiphase medium consisting of pure ice, gas bubbles, brine pockets, salt crystals, and sediments
33 (Hunke et al., 2011). In the last decades, the length of the Arctic ice melt season has shown a significant positive trend (Markus
34 et al., 2009), and the Arctic ice cover has experienced a transition from predominantly old ice to primarily first-year ice (Stroeve
35 and Notz, 2018; Tschudi et al., 2020). At the same time, in melting ice gas bubbles and brine pockets tend to become larger
36 (Light et al., 2003), and phase changes due to brine drainage and temperature result in variations in the volume of gas and
37 brine (Weeks and Ackley, 1986; Crabeck et al., 2019). Except for the above-mentioned factors, absorption of shortwave
38 radiation, synoptic weather, and surface melt pooling can also partly affect the ice microstructure. Therefore, the physical
39 properties of ice have changed and in the past 10 years the bulk density of summer Arctic sea ice has been lower than reported
40 in the 1990s due to increased ice porosity (Wang et al., 2020). Despite the changing ice microstructure having attracted
41 attention, there is still no quantitative description of its evolution and effect factors (Petrich and Eicken, 2010).

42 Gas bubbles and brine pockets, as dominant optical scatterers, directly influence the inherent optical properties (IOPs) of
43 sea ice (Grenfell, 1991; Perovich, 2003). IOPs include scattering and absorption coefficients and information about the phase
44 function of the domain. The varying IOPs of ice have attracted attention due to their important role in the process of light
45 penetration in ice. Light et al. (2008) and Katlein et al. (2019; 2021) demonstrated clear different IOPs in sea ice of different
46 depths. The differences in the IOPs between first-year ice and multiyear ice have been ascertained in many observations (e.g.,
47 Light et al., 2015; Grenfell et al., 2006). There are also some differences in the bulk IOPs of first-year ice because of the
48 different stages of melting (Veyssi  re et al., 2022). However, the available observed or estimated ice IOPs were rare, which
49 resulted in quantitative knowledge of the progression of the sea ice IOPs and their influencing factors was still absent (light et
50 al. 2015). Even in the latest studies and sea ice models, IOPs are set as constants based on previous field observations (e.g.,
51 Briegleb & Light, 2007), which is somewhat in contrast to the reality in the Arctic Ocean.

52 Changes in ice microstructure or IOPs are especially important for the energy budget of Arctic ice under the general
53 warming climate and decreasing ice age. The reason for this is their direct effect on ice apparent optical properties (AOPs),
54 which influence the partitioning of radiation in the Arctic by various feedback processes. However, the observed relationships
55 between ice microstructure, IOPs, and AOPs are rare in the available literature. Parameterization proposed by Grenfell (1991)
56 was the most widely used method to estimate the response of ice IOPs to microstructure. Due to the lack of detailed, observed
57 ice microstructure, this method was usually used to build models (e.g., Hamre, 2004; Light et al., 2004; Yu et al., 2022). In the
58 latest MOSAiC expedition during 2019-2020, Smith et al. (2022) observed the formation of a porous surface layer (i.e. surface

59 scattering layer, SSL) of sea ice and its enhancement on ice albedo. Macfarlane et al. (2023) further in detail described the
60 microstructure of SSL using X-ray tomography and its effects on ice optical properties. They are the first to link ice
61 microstructure and optical properties by field observations.

62 In this study, *in situ* observations of the physical properties of summer Arctic sea ice during the Chinese National Arctic
63 Research Expeditions (CHINARE) from 2008 to 2016 were employed as input data. Variations of the microstructure and the
64 IOPs of Arctic sea ice are presented. Also shown are their quantitative effects on the radiation budget. Applying these varying
65 IOPs to satellite-observed sea ice conditions has allowed us to estimate the role of ice microstructure in the radiation budget
66 in the Arctic basin scale.

67 **2 Data and method**

68 **2.1 Arctic sea ice coring**

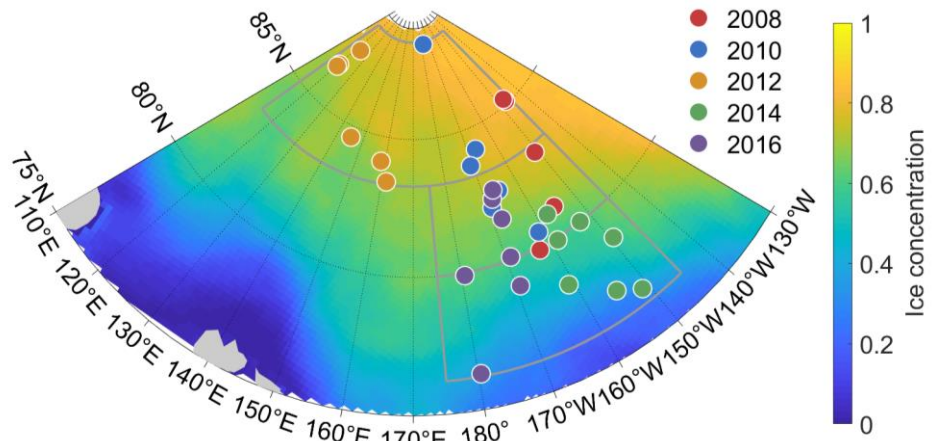
69 The Arctic sea ice cores were sampled in the Pacific sector of the Arctic Ocean during summer cruises of the CHINARE
70 program from 2008 to 2016 (Figure 1). The ice cores in each year were composed of different numbers of first-year ice and
71 multiyear ice with thicknesses from 0.6 to 1.9 m. Detailed volume fractions of the gas bubbles and brine pockets (V_a , V_b) in
72 the ice cores were given by Wang et al. (2020). The mean sampling date of ice cores was Aug. 20 \pm 8 days, when the ice had
73 been melting for a while (\sim 59 days) and had not yet begun to freeze according to the melting onset data from NASA. According
74 to previous observations, SSL of sea ice can be re-formed within a couple of days after removal (Smith et al., 2022). There are
75 no clear temporal changes in the microstructure of surface ice in the entire July (Macfarlane et al., 2023). Furthermore, the ice
76 surface melt rate in August was only \sim 1/10 of that in July (Perovich, 2003; Nicolaus et al., 2021). That is, it is expected that
77 the microstructure of the ice surface was similar in the mid- and late-melting seasons that cover the sampling dates of the
78 present ice cores. Therefore, the short-term temporal variability of ice cores was expected not to affect their surface ice
79 microstructure.

80 To further reduce the impact of temporal variations in the ice cores on the ice microstructure, we preprocessed the ice
81 core data. The ice cores in each year were allocated different weights according to their sampling date. The weight (w) of ice
82 cores in affecting period (D) can be obtained according to the Cressman method: $w = \frac{D^2 - d^2}{D^2 + d^2}$, where d is the number of days
83 from the mean sampling date. Then the weighted mean of ice properties was $\bar{x} = \frac{\sum_{i=1}^n w_i x_i}{\sum_{i=1}^n w_i}$. D was set to 30 days because the
84 weighted mean values and deviations were nearly unaffected when the D was over 30 days. In the following analyses, the
85 mean values of each year refer to the weighted ones. After the preprocessing, the deviation of melting days in a single year

86 was reduced by ~50.5%. As for the spatial variations in the ice cores, it is difficult for field observations to avoid the effects
87 of spatial variations. Therefore, related studies have generally ignored the effects of sampling locations on the statistics (e.g.
88 Carnat et al., 2013; Frantz et al., 2019; Katlein et al., 2019; Light et al., 2022). Related discussion about the temporal and
89 spatial variations can be found in Section 4.2.

90 A typical undeformed sea ice floe consists texturally of three layers due to its growth conditions (Tucker et al., 1992).
91 The first two layers are relatively thin and consist of a granular layer and a transition layer, and the lowest layer generally
92 consists of columnar ice. The ice texture controls the ice microstructure (Crabeck et al., 2016). Thus, the development of gas
93 bubbles, brine pockets, and IOPs in the three ice layers is different. Analogous to the parameterization of the Los Alamos sea
94 ice model (CICE; Briegleb & Light, 2007), Each ice core was evenly divided into 10 layers. The top (1/10) layer of an ice core
95 was defined as the top layer (TL), the second layer (2/10) was the drained layer (DL), and layers 4–10/10 collectively
96 constituted the internal layer (IL). Note that the surface scattering layer (SSL) and part of the DL were mixed in the TL and
97 could not be separated completely. Layer 3/10 was also a mixture of a DL and IL, and is therefore neglected in the following
98 analysis.

99



100

101 Figure 1. Locations of the sampled ice cores during CHINARE cruises. The ice cores were assorted into three parts according to latitude and
102 ice concentration. Their quantities were nearly the same in each zone. The ice concentration in the base map was the mean in August from
103 2008 to 2016.

104 2.2 Sea ice optics modeling

105 The IOPs of sea ice, including the scattering coefficient, σ , absorption coefficient, κ , and asymmetry parameter, g , can be
106 determined directly from the ice microstructure. Following the theory of Grenfell (1991), scattering in ice is caused by gas
107 bubbles and brine pockets, and absorption is caused by brine pockets and pure ice. This parameterization has been proved by
108 extensive observations (e.g., Light et al., 2004; Smedley et al., 2020). The IOPs of sea ice can be obtained from the sum of the

109 scatterers weighted by their relative volumes as:

110 $\sigma = \sigma_a + \sigma_b = \int_{r_{\min}}^{r_{\max}} \pi r_a^2 Q_a^{\text{sca}} N_a(r) dr + \int_{l_{\min}}^{l_{\max}} \pi r_b^2 Q_b^{\text{sca}} N_b(l) dl$ (1)

111 $\kappa = \kappa_i + \kappa_b = k_i V_i + \int_{l_{\min}}^{l_{\max}} \pi r_b^2 Q_b^{\text{abs}} N_b(l) dl$ (2)

112 $g = \frac{g_a \sigma_a + g_b \sigma_b}{\sigma}$ (3)

113 In these equations, the subscripts a and b represent gas bubbles and brine pockets, respectively, r is their radius (or equivalent
 114 radius), and l is the length of the brine pockets. Q^{sca} and Q^{abs} are the scattering and absorption efficiencies, respectively, which
 115 can be calculated using Mie theory. N is the size distribution function, subscript i represents pure ice, and $V_i = 1 - V_a - V_b$ is its
 116 volume fraction. The values of these parameters are summarized in Table 1. Brine pockets longer than 0.03 mm are modeled
 117 as cylinders rather than spheres (Light et al. 2003). The conversion function from Grenfell & Warren (1999) is employed to
 118 represent hexagon columns as spheres with the same optical properties. Besides, Q^{abs} and Q^{sca} in the required size range are
 119 obtained using their effective radii, which are calculated according to Hansen & Travis (1974).

120

121 Table 1. Parameters used in the radiation transfer model in Arctic summer and their sources

Parameter	Reference(s)
refractive index of gas bubbles	Light et al. (2004)
refractive index of brine pocket	Smith and Baker (1981)
N_a, N_b	Light et al. (2003)
k_i	Grenfell and Perovich (1981)
g_a, g_b	Light et al. (2004)
$r_{\min} = 0.5 \text{ mm}, r_{\max} = 2 \text{ mm}$	Grenfell (1983); Frantz et al. (2019)
$l_{\min} = 1 \text{ mm}, l_{\max} = 20 \text{ mm}$	Light et al. (2003); Frantz et al. (2019)

122

123 The Delta-Eddington multiple scattering model, where the constant IOPs from Briegleb & Light (2007) were replaced by
 124 the modeled IOPs, was employed to estimate the apparent optical properties (AOPs: albedo α_λ , transmittance T_λ , and
 125 absorptivity A_λ) of the ice at the sampling sites (Yu et al., 2022). This radiative transfer model was commonly used, and its
 126 accuracies were widely accepted. The integrated albedo (α_B), transmittance (T_B), and absorptivity (A_B) were calculated by
 127 integrating the spectral values over the band of the incident solar radiation, F_0 as:

128 $X_B = \frac{\int_{\lambda_1}^{\lambda_2} X_\lambda F_0(\lambda) d\lambda}{\int_{\lambda_1}^{\lambda_2} F_0(\lambda) d\lambda}, X = \alpha, T, A,$ (4)

129 In the following sections, the integrated absorption coefficient, κ_B , was also derived by this equation, following CICE
 130 (Briegleb & Light, 2007). Considering the generally cloudy weather in Arctic summer, the incident solar irradiance under an

131 overcast sky in August from Grenfell & Perovich (2008) was chosen as the default value for F_0 . The studied wavelength band
132 was set as the photosynthetically active band, i.e. $\lambda_1 = 400$ nm and $\lambda_2 = 700$ nm.

133 **2.3 Arctic-wide up-scaling**

134 To conduct an up-scaling analysis of the radiative budget of the Arctic sea ice cover based on observations of the ice
135 microstructure in the Pacific sector, we used representative basin-scale sea ice data to estimate the variations in the distribution
136 of radiation fluxes in summer during 2008-2016. The sea ice concentration (C) was provided by the National Snow and Ice
137 Data Center (NSIDC) (DiGirolamo et al., 2022), the sea ice thickness was based on CryoSat-2/SMOS data fusion (Ricker et
138 al., 2017), and the downward shortwave radiation flux at the surface (E_d) was obtained from the European Centre for Medium-
139 Range Weather Forecasts (ECMWF). The latter two datasets were interpolated to a 25 km NSIDC Polar Stereographic grid.
140 Then, the mean radiation fluxes and ice concentrations from July to September from 2008 to 2016 were set as the representative
141 values in summer. Due to the limitation of satellite remote-sensing data of summer ice thickness, the representative thickness
142 was estimated according to the mean value in October from 2011 to 2016, together with the growth rate estimated by Kwok
143 and Cunningham (2016). Then, representative ice thickness can be obtained. These gridded ice thickness and IOPs profiles from
144 ice cores were inputted in the radiative transfer model to estimate the ice AOPs. From all these data sets and the derived
145 parameters, the reflected, absorbed, and transmitted radiation flux by Arctic sea ice were calculated as $E_r = E_d \cdot C \cdot \alpha_B$, $E_a =$
146 $E_d \cdot C \cdot A_B$, and $E_t = E_d \cdot C \cdot T_B$, respectively.

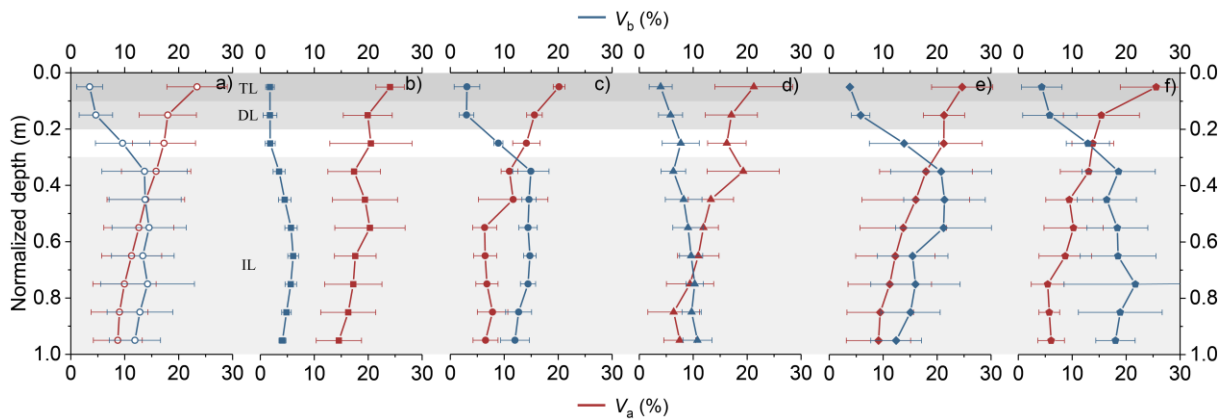
147 **3 Results**

148 **3.1 Microstructure of the ice cores**

149 There were different variation trends in the volume fraction of gas bubbles and brine pockets (V_a , V_b) as a function of ice
150 core depth (Figure 2). The upper granular ice was typically bubbly, associated with the drainage of brines, and the interior
151 columnar ice is usually depleted in gas bubbles (Cole et al., 2004). Thus, a significantly different V_a could be seen (Analysis
152 of variance (ANOVA), $P < 0.01$) with a decreasing trend along depth (Pearson correlation coefficient, $r = -0.97$, $P < 0.01$).
153 The mean V_a of the TL, DL, and IL for all ice cores was $23.4 \pm 5.6\%$, $17.9 \pm 5.3\%$, and $11.6 \pm 5.9\%$, respectively. These values
154 are similar to the observations made by Eicken et al. (1995) where V_a decreased from $> 20\%$ at the top to $< 5\%$ at the bottom
155 for summer Arctic sea ice.

156 The different V_b between layers was significant (ANOVA, $P < 0.01$). The drainage of brine resulted in a relatively small
157 V_b of TL, with a mean of $3.5 \pm 2.4\%$, while it was $4.6 \pm 3.1\%$ and $13.5 \pm 6.7\%$ in the other two layers, respectively (Figure
158 2a). $V_b = 5\%$ is usually chosen as a threshold where discrete brine inclusions start to connect and the columnar ice is permeable

159 enough to enable drainage (Carnat et al., 2013). Thus, the ice cores in the present study have been melting for some time,
 160 agreeing with the sampling season during CHINARE. Most V_b profiles had a maximum in the middle depth, except for the ice
 161 cores in 2012 (Figure 2d). This can be explained by the later sampling date in 2012 relative to the other years by about 10 days,
 162 which resulted in enhanced brine drainage. Furthermore, the shape of the V_b profile was also associated with the ice age (Notz
 163 and Worster, 2009). Compared with the ice cores in 2010, although the ice cores in 2016 had similar sampling dates (one day
 164 difference), the maximum position of V_b in 2016 was lower than in 2010 (Figure 2c, f). This was because all ice cores in 2010
 165 were sampled from first-year ice, and the ice cores in 2016 were comprised of first-year ice and multiyear ice (Wang et al.,
 166 2020).



167

168 Figure 2. Profiles of V_a and V_b against normalized depth in (a) the whole study period, (b) 2008, (c) 2010, (d) 2012, (e) 2014, and (f) 2016.
 169 The error bars show the standard deviation from the mean of the results. The shady areas represent the ice layer structure.

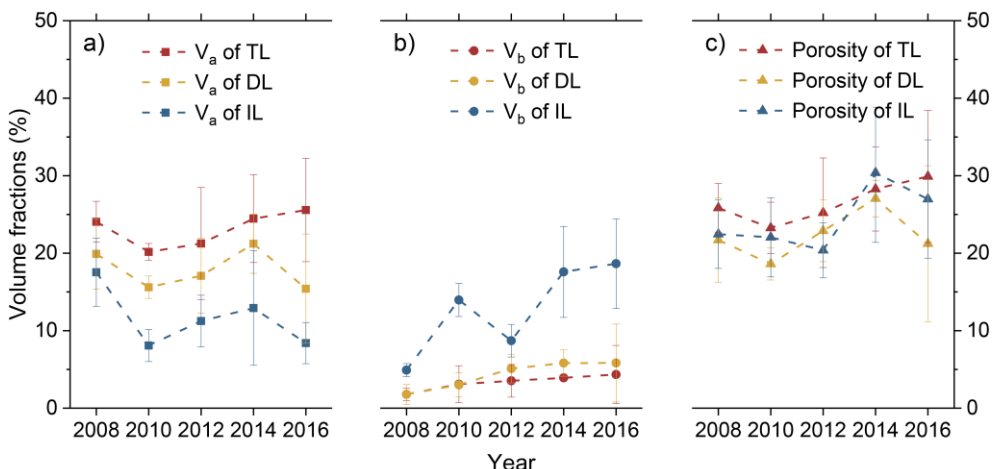
170

171 In addition to the different variations in V_a and V_b with depth, the annual variations in each layer were also different
 172 (Figure 3a). V_a was relatively small in the TL of 2010 because all ice cores were sampled from first-year ice (Wang et al.,
 173 2020). The quantities of first-year ice cores were similar to the amount of multiyear ice cores in the other years. The variation
 174 in V_a of TL between years was statistically insignificant (ANOVA, $P > 0.1$). This indicated that the melting process of the ice
 175 surfaces of the cores in different years was not different significantly. Contrary to the TL, the V_a in the IL was different
 176 significantly (ANOVA, $P < 0.05$). Compared with 2008, the mean V_a of IL in 2016 decreased by 9.1%. The V_a values of DL
 177 were relatively stable and did not show significant variations in the study period.

178 Things were different for V_b and ice porosity. There were increases in the mean V_b of all three ice layers (Figure 3b).
 179 Furthermore, the increases of mean V_b in the IL were statistically significant ($r = 0.84$, $P < 0.1$; ANOVA, $P < 0.01$). From 2008
 180 to 2016, the increase in the mean V_b of IL was 13%. Simultaneously, the ice salinity of the IL decreased (Figure S1), which
 181 agreed well with the observed and modeled results with warming conditions (e.g., Vancoppenolle et al., 2009). From the
 182 combined effects of changing V_a and V_b , there are no significant differences in the porosity of three layers (ANOVA, $P > 0.1$).

183 Furthermore, the developments of porosity in the three layers are also similar (Figure 3c). Among the three layers, the statistical
 184 significance of changing porosity of IL between years was relatively good (ANOVA, $P < 0.1$).

185

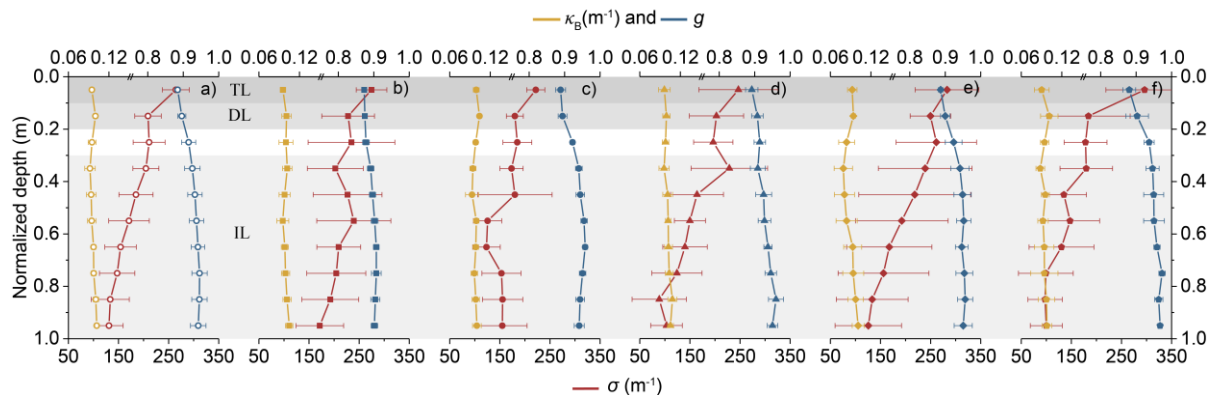


186
 187 Figure 3. Variations in (a) V_a , (b) V_b , and (c) the porosity of the TL, DL, and IL of the ice cores during 2008-2016. The error bars show the
 188 standard deviation for each year.

189 **3.2 Variations in the IOPs of the ice cores**

190 The mean scattering coefficient, σ , of the TL, DL, and IL for all ice cores was $264.5 \pm 26.7 \text{ m}^{-1}$, $208.9 \pm 26.5 \text{ m}^{-1}$, and
 191 $160.9 \pm 33.3 \text{ m}^{-1}$, respectively (Figure 4a). There was a significant decreasing tendency along with depth in the mean σ of all
 192 ice cores ($r = -0.97$, $P < 0.01$; ANOVA, $P < 0.01$), associated with a decreasing volume of gas bubbles (Figure 2). Although
 193 the V_b values of the ice cores increased clearly with depth, their effects on ice σ were covered by the decreasing V_a . The reason
 194 for this was that the refractive indices of brine pockets and pure ice are close (Smith and Baker, 1981; Grenfell and Perovich,
 195 1981), which results in the effects of brine pockets on ice σ were relatively weak than the gas bubble.

196 The vertical variations in κ_B and g were not clear as seen for σ because they depend on V_i and V_b/V_a , respectively. Due to
 197 the effects of the ice porosity ($V_a + V_b$), κ_B didn't show a statistically significant trend with depth (ANOVA, $P > 0.1$), which
 198 varied in the range 0.09 – 0.1 m^{-1} . The mean value of g was 0.93 except in 2008 (which was $g = 0.89$), and it significantly
 199 increased with depth ($r = 0.91$, $P < 0.01$; ANOVA, $P < 0.01$). This value is similar to the commonly used one; for example,
 200 the previous typical range of g was from 0.86 to 0.99 (e.g., Ehn et al., 2008), and 0.94 was often adopted for computational
 201 efficiency in models (Light et al., 2008). We note that the volume of brine pockets in ice cores of 2008 is relatively small,
 202 which was a reason for the different values of g found here.



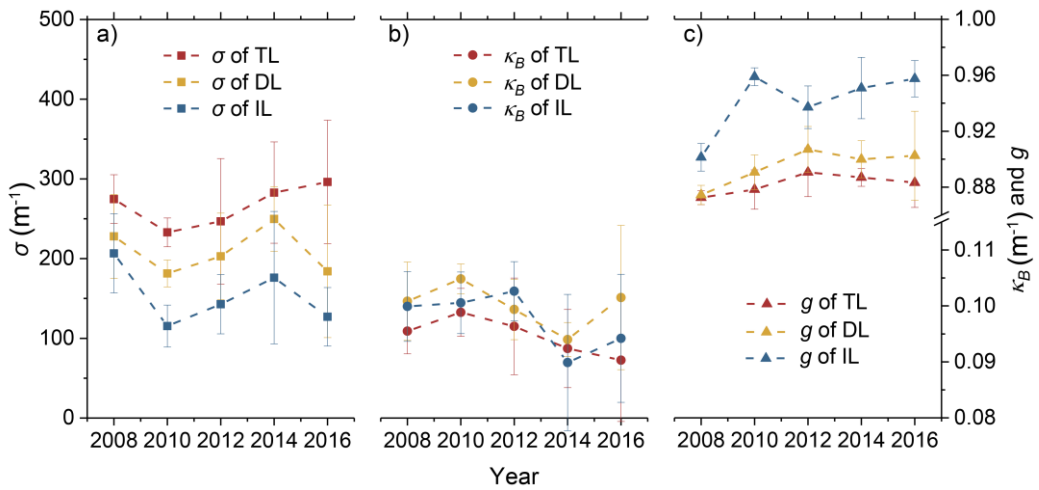
203
204 Figure 4. IOP profiles of ice cores against normalized depth in (a) the whole study period, (b) 2008, (c) 2010, (d) 2012, (e) 2014, and (f)
205 2016. The error bars show the standard deviation from the mean of the results.

206

207 The annual mean IOPs of the TL, DL, and IL of the ice cores are shown in Figure 5. As shown in Figure 5a, the variations
208 in σ of the TL, DL, and IL were different. The variation in σ of the TL between years was statistically insignificant (ANOVA,
209 $P > 0.1$), which reveals the relatively stable scattering ability of the ice surface. Things were different for IL, there were
210 statistically significant variations in their σ between years (ANOVA, $P < 0.05$). Compared with 2008, the σ of the IL in 2016
211 decreased by 38.4% due to the decreased V_a (Figure 3). The overall variations in the σ of the DL were similar to that seen in
212 the IL. Whereas, the former variations were not as clear as the latter due to ongoing drainage, and were not significant (ANOVA,
213 $P > 0.1$).

214 There were no statistically significant differences in the integrated absorption coefficient, κ_B , of the TL, DL, and IL
215 (ANOVA, $P > 0.1$), indicating the absorptivity of ice in different depths is similar. Furthermore, the developments of κ_B in the
216 three layers are similar ($\sim 0.001/\text{year}$, Figure 5b). Among the three layers, the statistical significance of changing κ_B of IL
217 between years was relatively better (ANOVA, $P < 0.05$) than TL and DL. As shown in Figure 5c, the values of g of the TL and
218 DL were nearly constant. Because their values of V_b were sufficiently small and similar due to drainage (Figure 3b), their
219 values of g are mainly attributed to gas bubbles. In contrast, the g of IL varied significantly (ANOVA, $P < 0.01$). The values
220 of g of the IL increased by 5% with increasing V_b in the study years (Figure 3b).

221



222

223 Figure 5. Annual (a) σ , (b) κ_B , and (c) g for the TL, DL, and IL of the ice cores from 2008 to 2016. The error bars show the standard deviation
224 in each year.

225

226 3.3 Variations in the AOPs of the ice cores

227 Having seen that the IOP profiles of the sea ice were not constant in the different years (Figure 5), a more important
228 question is how these changes affected the AOPs. The radiative transfer model was employed here to estimate the AOPs of
229 sampling sites, as shown in Figure 6. Note that the AOPs here were calculated based on the level ice. Surface properties, such
230 as a snow layer or melt ponds, were not considered here, because the focus was on the effects of the ice microstructure on their
231 AOPs. The results obtained with the same IOPs profiles but for a constant reference ice thickness (1 m) are also presented to
232 quantify the contributions from the ice microstructure and thickness separately. This reference thickness was chosen to study
233 the vertical structure relation to the surface and bottom and compare the samples with different thicknesses. This doesn't affect
234 the trends in Fig 6.

235 It can be seen from Figure 6a that the thickness of ice cores decreased in study years with a statistically significant trend
236 ($r = -0.89, P < 0.05$) and variations (ANOVA, $P < 0.05$). The values of α_B changed because of the effects of the ice IOPs and
237 thickness (Figure 6b). The variations in mean α_B during 2008-2014 were similar to those in the σ of the TL and DL. In 2016,
238 the mean α_B decreased due to the decreasing ice thickness. As a result, there are no statistically significant variations in α_B
239 between years (ANOVA, $P > 0.1$). This was different from the remote-sensing results (-0.05 per decade from 1982 to 2009) of
240 Lei et al. (2016). Part of the reason for this was the direct factor that reduces the annual ice albedo is not the ice microstructure
241 but rather the surface conditions. Eicken et al. (2004) and Landy et al. (2015) reported that the evolution of melt ponds on the
242 ice surface could explain 85% of the variance in the summer ice albedo.

243 Different from α_B , annual variations in T_B and A_B were significant (ANOVA, $P < 0.05$). The T_B (A_B) tended to increase

(decrease) with years (Figure 6c). The mean value of T_B in 2016 was over treble of that in 2008. Meanwhile, A_B decreased by about 19.5% from 2008 to 2016. Furthermore, the change of A_B in the study years was lower than the actual change in the ice thickness (-35.0%). Thus, the difference, $23.8\% \left(\frac{1-19.5\%}{1-35.0\%} - 1 \right)$, was attributed to an increase in the absorbed solar energy per unit volume of sea ice. This result does match the findings of Light et al. (2015), which showed that the thickness of first-year ice was less by 13.3% than multiyear ice (1.3 m vs. 1.5 m, respectively). However, the radiation absorbed by the former was less by 2% than the latter. In other words, the solar energy absorbed by a unit volume of first-year ice was greater than multiyear ice by 12.5%.

To make a direct comparison with the above variations, we considered a constant ice thickness, finding no clear changes in α_B (Figure 6b). Meanwhile, the variations in T_B and A_B were different clearly with similar overall trends (dashed lines in Figure 6c). T_B increased from 0.03 to 0.07 from 2008 to 2016, accounting for about 33.1% of the real change ratio with changing thickness. Thus, the changing microstructure of the melting ice resulted in an increased transmittance that was independent of the ice thickness. A similar result was observed in the laboratory, where the changing ice microstructure during the warming process (no decrease in thickness) increased the ice transmittance (Light et al., 2004). Different from T_B and A_B , whether the thickness was accounted for or not, the variations in α_B were hardly affected. This demonstrated that the present variations in ice thickness had more effects on the ice T_B and A_B than α_B .

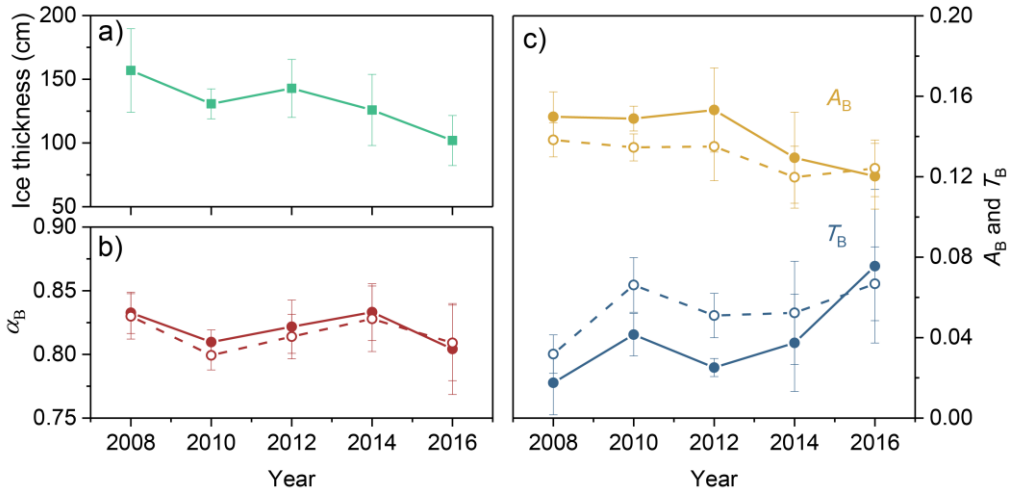


Figure 6. (a) Thickness and (b, c) estimated AOPs of the ice cores from 2008 to 2016. Also shown as dashed lines are the AOPs with the same IOPs and constant thickness (1 m). The error bars show the standard deviation in each year.

3.4 Arctic-wide estimation

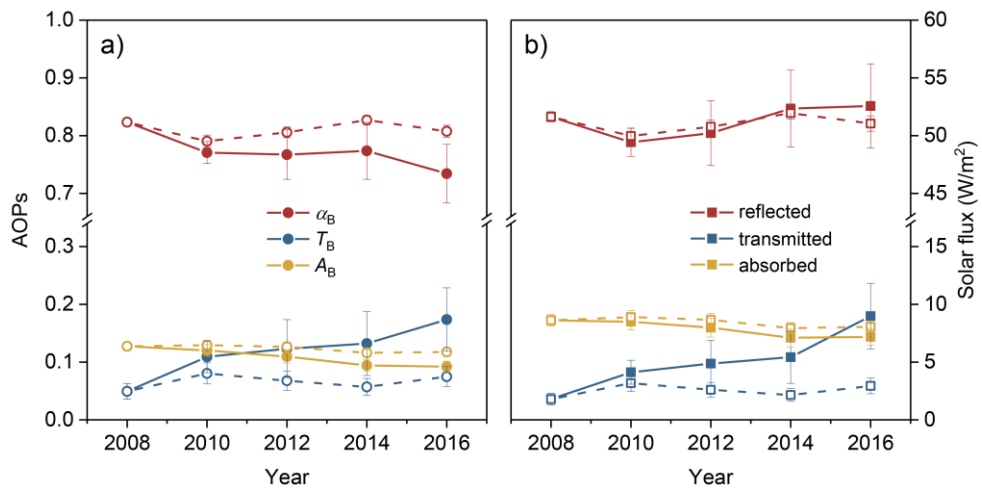
It may be interesting to estimate the quantitative effects of varying IOPs on the radiation distribution of the Arctic with a real ice thickness field, we expand the variations of the ice cores (Figure 5) to an Arctic-wide scale under the following

266 assumptions. 1), the IOPs of Arctic ice can be represented by our ice cores data. They are taken as constant, and seasonal and
267 spatial differences are ignored. This is justified since such a hypothesis has been widely used (e.g., Briegleb and Light, 2007).
268 2), a decreasing trend of -5.8 cm yr^{-1} in ice thickness according to Lindsay and Schweiger (2015) was adopted to get a general
269 view of the contributions of the changing ice thickness on the radiation budget. The representative basin-scale sea ice and
270 radiation data in summer (see Section 2.3) were used here to estimate the variations in the distribution of radiation fluxes.

271 With the combined effects of the changing microstructure and thickness of ice, Arctic-wide variations in the mean α_B , T_B ,
272 and A_B were statistically significant (ANOVA, $P < 0.01$) and clearer than those in Figure 6 (Figure 7a), especially the overall
273 trends of the mean T_B ($r = 0.95$, $P < 0.01$) and A_B ($r = -0.98$, $P < 0.01$) of ice. Although the mean α_B decreased from 2008 to
274 2016, there was not much change in reflected solar flux (E_r), about 51.2 W m^{-2} during the study years (Figure 7b). This was
275 resulted from that the decreasing α_B was largely provided by marginal ice zones. The decreasing rate of α_B in regions with ice
276 thicknesses $< 1 \text{ m}$ (equivalent to 16.4% of the entire ice area) was over 1.6 times the rate of the entire ice cover (Figure S2).
277 With the retreat of sea ice, the reflected flux of the marginal zone contributes less and less to the reflected flux of the entire ice
278 cover.

279 Different from E_r , the overall trends of transmitted (E_t) and absorbed solar flux (E_a) were clear under the combined effects
280 of the changing microstructure and ice thickness. The mean E_t was significantly different between years (ANOVA, $P < 0.01$),
281 and increased from 1.8 W m^{-2} to 9.0 W m^{-2} from 2008 to 2016 significantly ($r = 0.93$, $P < 0.05$, Figure 7b). Most of the increase
282 in E_t is ascribed to thin ice in marginal ice zones (ice thicknesses $< 1 \text{ m}$), which contributed 51.8% of the increasing E_t from
283 2008 to 2016 (Figure 8a–e). Meanwhile, variations in transmitted solar radiation E_a were significant (ANOVA, $P < 0.01$). The
284 E_a decreased from 8.6 W m^{-2} in 2008 to 7.2 W m^{-2} in 2016 significantly ($r = -0.94$, $P < 0.05$). As the decrease in ice volume
285 from 2008 to 2016 was 32.2%, the solar energy absorbed by a unit volume of sea ice increased by 23.4% on the Arctic scale.

286



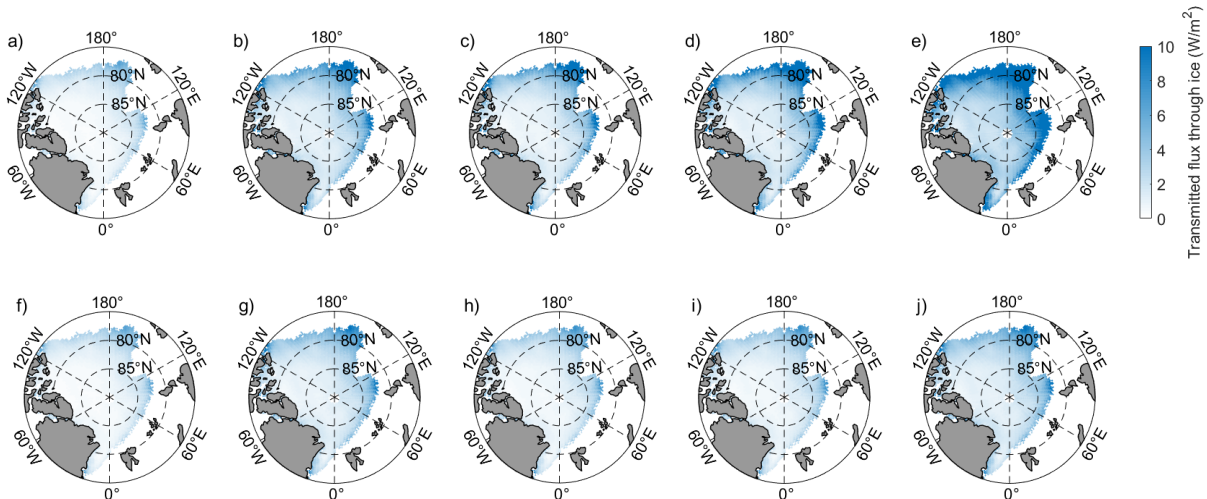
287

288 Figure 7. Arctic-wide variations in the mean (a) AOPs of ice and (b) solar flux distribution during 2008-2016. Also shown as dashed lines
289 are the AOPs and fluxes with the same IOPs and constant thickness field. The error bars show the standard deviation in each year.

290

291 When the ice thickness was set as a constant, variations in the mean AOPs were different, which resulted in differences
292 in the solar flux (dashed lines in Figure 7b). Among them, differences in the reflected flux E_r were relatively small. Meanwhile,
293 the mean E_t increased from 1.8 W m^{-2} in 2008 to 2.9 W m^{-2} in 2016, with no significant trend. E_a decreased from 8.6 W m^{-2} to
294 8.0 W m^{-2} in the same period. These changes corresponded to 16.0% and 39.3% of the combined effects of the ice IOPs and
295 thickness, respectively, from 2008 to 2016. Furthermore, marginal ice zones with ice thicknesses $< 1 \text{ m}$ still contributed 38.5%
296 of the increasing E_t from 2008 to 2016 (Figure 8f-j). This value was about 74.3% of the rate of the combined effects of the
297 changing IOPs and thickness of ice. In other words, the same changes in the ice microstructure had more effects on the T_B of
298 thin sea ice, and these effects were clearer than those resulting from general decreasing ice thickness.

299



300

302 Figure 8. Distribution of transmitted solar radiation through sea ice in the summers of 2008 to 2016 when the sea ice thickness was set (a–
303 e) to decrease and (f–j) to a constant value. Only flux that penetrated through the sea ice is considered in this map.

304 **4 Discussion**305 **4.1 Comparisons with IOP measurements**

306 In Section 3.2, we estimated the ice IOPs according to the observed ice physics and structural-optical theory. Other
307 methods were used to estimate ice IOPs in previous studies. In this section, we compare the ice scattering coefficient, the most
308 variable value among IOPs, determined in the present study with previous results (Figure 9). It is difficult for us to consider
309 the potential affecting factors because the variations in σ were still unclear. So, we pay more attention to the comparison of σ
310 range. The differences in wavelength bands were ignored in the comparisons because σ was nearly wavelength-independent.

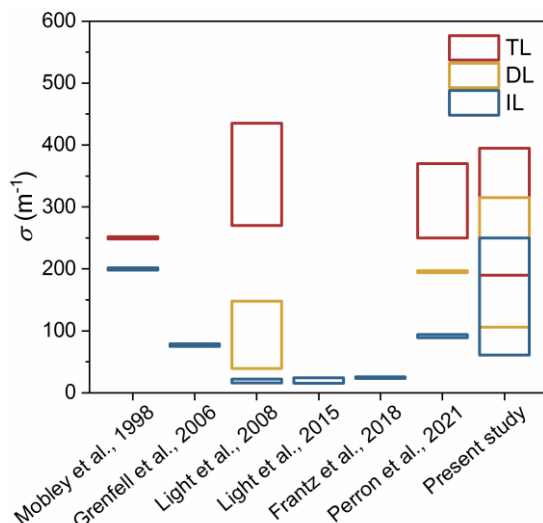
311 It is clear from Figure 9 that the range of σ of the present study covered the majority of previous results. The derived
312 values of σ for the SSL and DL of melting bare ice in August ranged from 920 to 2,000 m⁻¹ and 40 to 150 m⁻¹, respectively
313 (Light et al., 2008). According to the layer structure, wherein the TL was composed of a 5 cm SSL and the others were DLs,
314 the bulk σ of the TL in Light et al. (2008) ranged from 270 to 435 m⁻¹. This result was slightly higher than our results. The
315 results of Mobley et al. (1998) and Perron et al. (2021) agree with our range. The σ of the DL in Perron et al. (2021) was in
316 our range, and the values of Light et al. (2008) were smaller than those in the present study.

317 Differences in the σ of the IL were clearer than in the TL and DL. The σ values of the IL of most our cores were relatively
318 larger than those of Light et al. (2008, 2015) and Frantz et al (2019). In these results, Light et al. (2008) estimated the σ using
319 the observed ice albedo and a three-layer structure with fixed thicknesses. The results of Light et al. (2015) and Frantz et al.
320 (2019) were obtained in a cold laboratory by simulating the radiative transport in subsections of sea ice. Meanwhile, the results
321 of Grenfell et al. (2006) and Perron et al. (2021) are close to the minimum of our range. The σ of ice in Grenfell et al., (2006)
322 was calculated from the ice extinction coefficient, and it was measured *in situ* using a diffuse reflectance probe in the Perron
323 et al. (2021). The values calculated by the same method as used in the present study by Mobley et al. (1998) were close to the
324 maximum of our range. Thus, it was expected that the differences in the IL's σ partly resulted from the different methods used
325 in the myriad studies.

326 One possible reason for the differences was the uncertainties in the ice microstructure introduced by brine loss during
327 measurement and segmenting. Thus, our V_a values of the IL are greater than the values derived from nondestructive methods
328 (e.g., Perron et al., 2021). As a result, the maximum underestimate of V_b was 15–25% and the maximum overestimate of V_a
329 was 96–160% when taking the uncertainties introduced by the measurements and brine drainage into account (Wang et al.,
330 2020). Taking the mean V_a and V_b of all ice cores as an example, these uncertainties overestimated the σ of the IL by 78 m⁻¹ at
331 most. Although brine loss during sampling and measurements introduced uncertainties to V_a and V_b , the methods used for
332 obtaining and measuring the ice cores during the CHINARE cruises were the same. Therefore, the uncertainties introduced by

333 the methodology hardly affected the changes seen in Figure 6 and Figure 7.

334



335

336 Figure 9. Comparison of the ice scattering coefficient in the present study to the published results for Arctic sea ice using various methods.
337 All comparison results have been scaled to the layer structure used in the current study according to their ice thicknesses.

338

339 Another source of difference is the distribution function of gas bubbles employed in the IOP parameterization. Many
340 distributions are obtained in a cold laboratory, where the ice temperature is not consistent with that in the summer Arctic. As
341 the refractive indices of brines and pure ice were similar, the distribution function of brine pockets had a smaller influence on
342 the ice IOPs than gas bubbles (Yu et al., 2022). Here, we tentatively adjusted the exponent of the distribution function of the
343 gas bubbles from its default value of -1.5 to -1, i.e., the fraction of small bubbles decreases, which coincides with warming ice
344 (Light et al., 2003). Then, the changed distribution function was used for 1 m thick ice with mean values of V_a and V_b for every
345 ice core. This change resulted in an uncertainty of $8 m^{-1}$ in the σ of each layer. These uncertainties did not alter the above
346 results and are considered acceptable.

347 Although brine loss and the difference in the distribution functions of gas bubbles introduced uncertainties in σ , they did
348 not affect the ice AOPs much. Considering a 1 m thick ice layer described by the mean physics of ice cores, the effects of the
349 former factor on the ice AOPs were less than 0.02. The uncertainties in α_B and T_B introduced by the latter factor were 0.005
350 and 0.002, respectively. Therefore, our estimated α_B range (0.76–0.87) agreed with the observed results of Light et al. (2008,
351 2015) and Grenfell et al. (2006). Meanwhile, the estimated T_B (0.01–0.1) was also in the corresponding observed ranges.

352 **4.2 On the potential interannual variations of the IOPs**

353 Extensive measurements of the IOPs of Arctic sea ice have been carried out, and some authors have noticed the seasonal
354 variations of the ice microstructure and IOPs (e.g., Light et al., 2008; Frantz et al., 2019; Katlein et al., 2021). However, if
355 there are interannual variations in sea ice IOPs are still not clear, although such changes in sea ice extent, thickness, and age
356 are evident. A lack of continuous IOP measurements is the primary reason. Compared with previous observations, the ice core
357 data in the present study were more appropriate for analyses on the potential interannual variations in ice IOPs because of their
358 long time span and consistencies in the sampling method, seasons, and sea areas. The reason we could not introduce other ice
359 core data (SHEBA, ICESCAPE, N-ICE, MOSAiC, etc.) into this study was that not only the differences in sampling seasons,
360 sites, and methods increase the dispersion in time and space during such an analysis, but also the lack of information about the
361 ice microstructure or essential physical properties will limit how much we can determine from such a comparison. We consider
362 the presented ice core data is the best possible estimate on the potential interannual variations at this time, while acknowledging
363 that further improvements of the data products are needed. Considering that sampling ice cores is a commonly used method
364 for *in situ* observations, with more suitable ice core data in the future, large-scale time series of ice IOPs may be obtained.

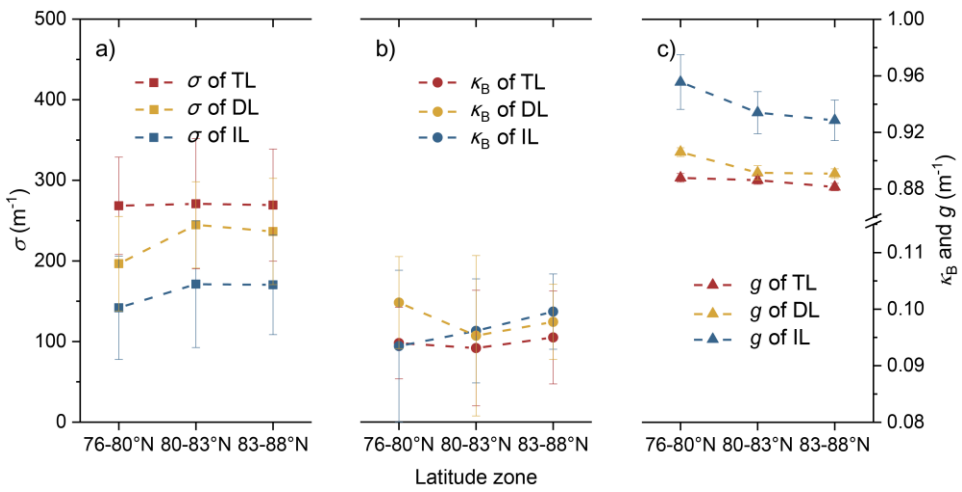
365 The ice cores used in the present study were sampled at different ice stations but not at the same floe (Figure 1). That is,
366 the data did not form a continuous observation in the strictest meaning. Thus, the variations shown in Section 3 can be regarded
367 as the combined effects from three parts, i.e. spatial, temporal, and interannual variations. To do the discussion of interannual
368 variability, it is necessary to first establish the spatial and temporal variability of ice cores. Figure 10 illustrates the different
369 IOPs of the ice cores in three latitude zones, which shows that there are spatial differences in the present ice core data. Among
370 the three IOPs, variations in σ are the clearest (up to 20%, Figure 10a). The differences in κ_B and g in the different latitude
371 zones were not more than 5% and 3%, respectively (Figure 10b, c). As a transition layer between the TL and IL, variations in
372 the IOPs of the DL were more discrete than in the other two layers. For now, we have little quantitative knowledge of the
373 progressions of the sea ice IOPs and their influencing factors in the available literature. In the following discussion, the σ was
374 set as the main content.

375 It can be seen from Figure 10a that there were no clear changes in the mean σ of TL in different latitude zones. Therefore,
376 we ignore the spatial variations in σ of TL. We further discuss its whole variations in different years. The variability of the ice
377 surface is directly related to the number of melt days. The melt days are affected by the radiation balance, water vapor, air
378 temperature, and other factors (Persson, 2012; Mortin et al., 2016; Crawford et al., 2018). Figure 11a shows the data obtained
379 from ECMWF, the downward longwave radiation was $300.2 \pm 4.0 \text{ W/m}^2$ at the surface during the study years with no
380 statistically significant trend ($r = -0.57$, $P > 0.1$). The total column vertically integrated water vapor was also similar ($11.9 \pm$

381 0.4 kg/m²) with no significant trend ($r = -0.58, P > 0.1$). Different from the surface radiation, we found the observed air
382 temperature increased at a speed of 0.14 °C/year ($r = 0.84, P < 0.1$, Figure 11a). This clear difference in the temperatures was
383 not an exception but a general circumstance in the Arctic during 2008–2016 (e.g., Collow et al., 2020). This could also be seen
384 in the reanalysis data of ECMWF, where the mean air temperature in the summer of the study area has been increasing gradually
385 (0.12 °C/year, $r = 0.84, P < 0.1$). With the effects of several factors, the melting days of sampling sites, which were calculated
386 according to the sampling date and melt onset from Markus et al. (2009), were 59 ± 7 days (Figure 11a). Their variation
387 between years was statistically insignificant (ANOVA, $P > 0.1$). In other words, there are no significant differences in the
388 surface melt of the ice cores in different years.

389 Previous observations demonstrated that ice surface melt was relatively weak in August (Perovich, 2003; Nicolaus et al.,
390 2021). Macfarlane et al. (2023) further found that the SSL microstructure of melting ice has no temporal changes. Meanwhile,
391 the differences in longwave radiation and vapor between sampling sites in single years were relatively small (Figure 11a). So,
392 it is expected that the scattering coefficient of TL also has no clear seasonal variations. Whereas, an increasing scattering in
393 the SSL during melt season was found in Light et al. (2008). This seems contrary to the findings of Macfarlane et al. (2023),
394 but it is not. As stated in Light et al. (2008), the observed increase in scattering represents not only an increased scattering in
395 a fixed depth layer but also an increased physical depth of the SSL or increased scattering of the next ice layer, because the
396 modeled layer thickness was fixed. What was the same in the two studies was approximately constant albedo (or reflectance).
397 This agrees with the similar albedo in Figure 6b of the present study, i.e. small seasonal differences don't affect the reflectivity
398 of bare ice. For now, there was no theoretical explanation or quantitative description of the evolution of the microstructure of
399 the ice surface during the melt (Petricch and Eicken, 2010). It can be seen from the present result, the increasing air temperature
400 seems not the predominant affecting factor in the late melting season. In short, it is expected that the effects of temporal
401 variations on the microstructure and IOPs of the ice surface were relatively small. Considering the whole variations in
402 microstructure (Figure 3) and IOPs (Figure 5) were not significant, there are no clear temporal, spatial, or interannual variations
403 in the ice surface of the present ice core data.

404



406 Figure 10. Different values of (a) σ , (b) κ_B , and (c) g for the TL, DL, and IL of the ice cores in the three latitude zones. The error bars show
407 the standard deviation in each latitude zone.

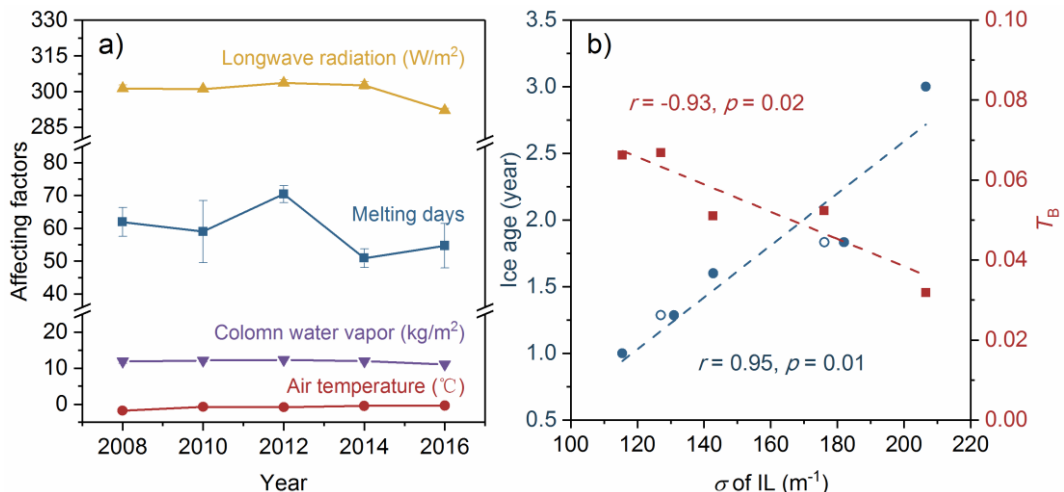
408

409 The σ of the IL is relatively constant during the entire melt season (Light et al., 2008). That's to say, the whole variations
410 in the ice interior layer didn't result from temporal factors. Meanwhile, the latitudinal differences in the σ of the IL are clear.
411 The σ of the ice IL in the low-latitude zone was relatively smaller than that in mid- or high-latitude zones (Figure 10a). This is
412 expected that the ice at lower latitudes is generally warmer earlier, which increases the brine inclusion size and connectivity
413 of ice. Then naturally reduced the ice scattering coefficient. The spatial variation of mean σ in the IL can be up to 30 m^{-1}
414 between low-latitude and mid- or high-latitude zones. This value was equivalent to 32.9% of the maximum of the whole
415 variation. This implied that the spatial and interannual variations in ice properties together result in the changing IOPs shown
416 in Figure 5. So, it is necessary to exclude the spatial variations before discussing the interannual changes of σ . According to
417 the propagation law of variation, the square of whole variations of IL- σ can be expressed as the square sum of their spatial
418 variations and interannual variations. For the convenience of calculation, we ignored the small difference IL- σ between mid-
419 and high-latitude zones. There are five and three cores in 2014 and 2016 sampled in the low-latitude zone, respectively.
420 According to the differences between ice cores from different years (whole variations, Figure 3) and different latitude zones
421 (spatial variations, Figure 10a), we correct the mean σ of the IL in 2014 from 176 m^{-1} to 182 m^{-1} . That's to say, the interannual
422 variations were larger than the whole variations by 6 m^{-1} . The value of 2016 was also corrected from 127 m^{-1} to 131 m^{-1}
423 accordingly. Then, variations among the corrected σ of the IL could be regarded as the result of the interannual factors.

424 Then, the corrected σ of the IL was used to discuss the interannual changes. Figure 11b shows the correlations among the
425 corrected σ of the IL, ice age, and T_B in study years. Also shown in circles were the uncorrected σ of IL in 2014 and 2016. Note
426 that T_B here is the result under the assumption of a constant ice thickness (dashed line in Figure 6c). The ice ages were obtained

427 according to fieldwork (Wang et al., 2020) and remote-sensing data (Tschudi et al., 2019). Because the ice age of each grid
 428 cell in the remote-sensing data is represented as the age of the oldest floe, once an ice core was distinguished as first-year ice
 429 in the fieldwork, the corresponding ice age was set as one year regardless of the remote-sensing data. The use of remote-
 430 sensing data is acceptable because the ice cores in this study were all sampled in large and thick floes for safe fieldwork. These
 431 floes were more likely older than the surrounding ice. Figure 11b demonstrates that the decrease in the σ of the IL is
 432 significantly correlated with changing ice age ($r = 0.95, P < 0.01$). In other words, the ice age largely manifested in the ice
 433 microstructure in the IL. A similar result was also observed i.e. the σ of the IL in the first-year ice was smaller than in multiyear
 434 ice (e.g. Light et al. 2015). This could also partly explain the spatial variations in the σ of the IL (Figure 10a) because sea ice
 435 in high-latitude zones was likely older than in the other zones (Stroeve and Notz, 2018). Furthermore, there are significant
 436 correlations between σ of the IL and ice T_B ($r = -0.93, P < 0.05$). That's to say, the changing ice age can be responsible for the
 437 modeled results of changing ice transmittance shown in Figure 7, even without any decrease in the ice thickness. One other
 438 thing to point out, the changing ice age seems to not affect the albedo of bare ice (Figure 6b). Light et al. (2022) suggest that
 439 the principal reason for this is the SSL shows invariance across location, decade, and ice age, which was confirmed by
 440 comparing data from MOSAiC (2019-2020) and SHEBA (1997-1998). Our results partly prove this view i.e. there are
 441 significant variations in the ice age but no significant variations in microstructure or IOPs of TL during 2008-2016.

442



443

444 Figure 11. (a) Changing melting days, surface downward longwave radiation flux, total column vertically-integrated water vapor, and
 445 observed air temperature at the sampling sites. The error bars show the standard deviation in each year. Some error bars are invisible
 446 because they are small enough. (b) Correlations among the σ of the IL with ice age and T_B . The circles denote the uncorrected data.

447

448 In summary, we didn't find significant variations in the IOPs of the ice top layer. Meanwhile, the differences in the IOPs

449 of the ice IL were related to interannual variations in the ice age. To our knowledge, this is the first study to link ice
450 microstructure and optical properties at interannual scales. Although these ice core data are not a time series in the strictest
451 meaning, they are still helpful for understanding the general effects of the scenario where the Arctic ice ages are decreasing.
452 Our results suggested that in this scenario, the σ values of the IL of summer ice tended to be smaller than before. It is expected
453 to lead to interannual trends of the ice microstructure and IOPs. Then, more solar radiation transmits into the ocean. The effects
454 of this process need more attention in future observations and simulations.

455 **4.3 Implications for the future Arctic**

456 Previous studies have reported that surface properties (snow, ponds, etc.) largely control the variations in the ice albedo
457 (Landy et al., 2015). The present results also asserted that variations in the ice's microstructure or IOPs had little effect on the
458 albedo of bare ice (< 2%), but they do play an important role in ice transmittance (Figure 6). With continued Arctic warming,
459 the summer ice age is on the decrease, and the ice microstructure and IOPs change accordingly, leading to an overall higher
460 ice transmittance. Furthermore, the transmitted solar energy affects the temperature of the upper ocean and results in further
461 melting of the bottom of sea ice (Timmermans, 2015). Along with the melting of ice, gas bubbles, and brine pockets change
462 simultaneously (Light et al., 2004), which affects the IOPs of ice in turn. Consequently, the sea ice is expected to become
463 thinner and more porous than before. This process has been seldom considered in previous studies. Related studies generally
464 regarded the surface properties and thickness of the ice as predictors for light transmittance (e.g., Katlein et al., 2015; Perovich
465 et al., 2020). The microstructure and morphological parameters of sea ice (e.g., thickness, extent, etc.) may together influence
466 the melting processes of Arctic sea ice.

467 For safe field observations, the ice core data used in this study were all sampled in large and thick floes. Therefore,
468 variations in the microstructure of the ice in marginal zones or under melt ponds cannot be addressed by this study. Light et al.
469 (2015) reported that the differences in the σ between the IL of ponded first-year ice and multiyear ice were larger than those
470 between bare first-year ice and multiyear ice. Therefore, the changes in the IOPs of the marginal ice zone were expected to be
471 more obvious than those found in the present results because the ice in marginal zones is more likely young and ponded (Rigor
472 and Wallace, 2004; Zhang et al., 2018). Furthermore, the same changes in the ice microstructure have more effects on the T_B
473 of thin sea ice (Section 3.4). Marginal ice zones, comprising 16.4% of the entire ice area, contributed 39.3% of the extra-
474 transmitted solar energy due to the changing ice microstructure from 2008 to 2016 (Figure 8). Both processes promote an
475 increase of transmitted flux through sea ice and ice bottom melting in marginal ice zones. Arndt & Nicolaus (2014) quantified
476 light transmittance through the sea ice into the ocean for all seasons as a function of variable sea ice types. The mean annual
477 trend was 1.5% per year, which mainly depended on the timing of melt onset. If the variations in the microstructure of bare

478 and ponded ice are taken into consideration, this trend is expected to increase. We suggest that future ice observations and
479 models should pay more attention to variations in the ice age, microstructure, and their effects, especially in marginal ice zones.

480 We want to emphasize the Arctic basin-scale analysis is a highly idealized investigation. To obtain a real distribution of
481 the transmitted solar radiation through sea ice in the Arctic basin scale in the summer is far more complicated and would
482 require a massive amount of ice core sampling collected simultaneously in various parts of the Arctic Ocean. Such field
483 expeditions cannot be arranged anytime soon in the future. We intend to provide one possible scenario of IOPs. We call for
484 further strengthening international collaborations to make possible a better understanding of the Arctic IOPs distribution.

485 **5 Conclusions**

486 This is the first study to link the ice microstructure, IOPs, and AOPs at interannual scales. Based on ice cores sampled
487 during the CHINARE expeditions (2008–2016), the variations in the IOPs of Arctic sea ice in summer due to the changing
488 microstructure of ice were modeled according to structural-optical theory. Variations in the AOPs and solar flux distribution
489 due to the changing IOPs in the summer Arctic were also estimated. Clear variations in the microstructure and IOPs of each
490 year (Figure 5) enabled us to construct a quantitative view of changes that the Arctic sea ice interior underwent in these years.

491 As a result of our study, there were no significant variations in the microstructure and IOPs of ice TL. This is related to
492 the stable melt days in study years. Because σ of the upper layers (TL and DL) mainly control the albedo of bare ice, the
493 variations in α_B between years were relatively small. Meanwhile, variations in the microstructure and IOPs of IL were
494 significant. These variations consist mainly of interannual factors and minor spatial factors. After excluding the effects of
495 spatial variations, we found these interannual variations in σ of ice IL were highly related to the changing ice ages. That's to
496 say, the ice age largely manifested in the ice microstructure of the IL. The changing σ of ice IL affects the ice transmittance
497 clearly. Furthermore, the same changes in the ice IOPs had more effects on the transmittance of the thin ice in marginal ice
498 zones.

499 Previous studies paid more attention to changing transmittance due to declining ice thickness. The present findings
500 demonstrated that the changing IOPs of interior ice derived from the ice microstructure could also alter the partitioning of solar
501 radiation in sea ice by itself. With continued Arctic warming, summer ice will become younger and more porous than before,
502 leading to more light reaching the upper ocean. This reminds us to pay more attention to the variations in the IOPs of interior
503 ice, especially ice with different ages.

505 *Acknowledgments.* We would like to thank Handling editor Dr. Marie Dumont and 4 anonymous reviewers. Their criticism and
506 constructive comments helped to improve this manuscript significantly. We are grateful to the NSIDC, Alfred Wegener Institute,
507 and ECMWF for providing the sea ice and radiation data. This work was financially supported by the National Key Research
508 and Development Program of China (Grant number 2018YFA0605901), the National Natural Science Foundation of China
509 (Grant numbers 41922045, 41906198, 41976219, and 41876213), and the Academy of Finland (Grant numbers 333889,
510 325363, and 317999). We also wish to acknowledge the crews of the R/V Xuelong for their fieldwork during CHINARE.

511 *Author contributions.* MY carried out the estimations and wrote the paper. RL, BL, and QW provided the ice core data. All
512 coauthors discussed the results and edited the manuscript.

513 *Data Availability Statement.* The sea ice and radiation data are available at <https://doi.org/10.5067/MPYG15WAA4WX>;
514 https://data.meereisportal.de/gallery/index_new.php?lang=en_US&ice-type=extent&active-tab1=measurement&active-tab2=thickness; <https://cds.climate.copernicus.eu/cdsapp#!/dataset/reanalysis-era5-single-levels-monthly-means?tab=form>. The
516 ice cores data applied in this work can be accessed in Wang et al. (2020).

517 *Competing interests.* The authors declare that they have no conflict of interest

518

519 **References:**

520 Arndt, S. and Nicolaus, M., 2014. Seasonal cycle and long-term trend of solar energy fluxes through
521 Arctic sea ice. *The Cryosphere*, 8 (6): 2219-2233. doi:10.5194/tc-8-2219-2014

522 Briegleb, B. P. and Light, B., 2007. A Delta-Eddington Multiple Scattering Parameterization for Solar
523 Radiation in the Sea Ice Component of the Community Climate System Model (No. NCAR/TN-
524 472+STR). University Corporation for Atmospheric Research. doi:10.5065/D6B27S71

525 Carnat, G. and Papakyriakou, T., et al., 2013. Investigations on physical and textural properties of Arctic
526 first-year sea ice in the Amundsen Gulf, Canada, November 2007 – June 2008 (IPY-CFL system
527 study). *Journal of Glaciology*, 59 (217): 819-837. doi:10.3189/2013JoG12J148

528 Cole, D. M. and Eicken, H., et al., 2004. Observations of banding in first-year Arctic sea ice. *Journal of*
529 *Geophysical Research: Oceans*, 109 (C8): n/a-n/a. doi:10.1029/2003JC001993

530 Collow, A. B. and Cullather, R. I., et al., 2020. Recent Arctic Ocean Surface Air Temperatures in
531 Atmospheric Reanalyses and Numerical Simulations. *Journal of Climate*, 33 (10): 4347-4367.
532 doi:10.1175/JCLI-D-19-0703.1

533 Comiso, J. C. and Parkinson, C. L., et al., 2008. Accelerated decline in the Arctic sea ice cover.
534 *Geophysical Research Letters*, 35 (1): L01703. doi:10.1029/2007GL031972

535 Crabeck, O. and Galley, R. J., et al., 2019. Evidence of Freezing Pressure in Sea Ice Discrete Brine
536 Inclusions and Its Impact on Aqueous - Gaseous Equilibrium. *Journal of Geophysical Research:*
537 *Oceans*, 124 (3): 1660-1678. doi:10.1029/2018JC014597

538 Crabeck, O. and Galley, R., et al., 2016. Imaging air volume fraction in sea ice using non-destructive X-
539 ray tomography. *The Cryosphere*, 10 (3): 1125-1145. doi:10.5194/tc-10-1125-2016

540 Crawford, A. D. and Horvath, S., et al., 2018. Modulation of Sea Ice Melt Onset and Retreat in the Laptev
541 Sea by the Timing of Snow Retreat in the West Siberian Plain. *Journal of Geophysical Research:*

542 Atmospheres, 123 (16): 8691-8707. doi:10.1029/2018JD028697

543 Dai, A. and Luo, D., et al., 2019. Arctic amplification is caused by sea-ice loss under increasing CO₂.
544 Nature Communications, 10 (1). doi:10.1038/s41467-018-07954-9

545 DiGirolamo, N. E. and Parkinson, C., et al., 2022. updated yearly. Sea Ice Concentrations from Nimbus-
546 7 SMMR and DMSP SSM/I-SSMIS Passive Microwave Data, Version 2. Boulder, Colorado USA.
547 NASA National Snow and Ice Data Center Distributed Active Archive Center..

548 Ehn, J. K. and Papakyriakou, T. N., et al., 2008. Inference of optical properties from radiation profiles
549 within melting landfast sea ice. Journal of Geophysical Research, 113: C09024.
550 doi:10.1029/2007JC004656

551 Eicken, H. and Grenfell, T. C., et al., 2004. Hydraulic controls of summer Arctic pack ice albedo. Journal
552 of Geophysical Research: Oceans, 109 (C08007): n/a-n/a. doi:10.1029/2003JC001989

553 Eicken, H. and Lensu, M., et al., 1995. Thickness, structure, and properties of level summer multiyear ice
554 in the Eurasian sector of the Arctic Ocean. Journal of Geophysical Research, 100 (C11): 22697-
555 22710. doi:10.1029/95JC02188

556 Frantz, C. M. and Light, B., et al., 2019. Physical and optical characteristics of heavily melted "rotten"
557 Arctic sea ice. The Cryosphere, 13 (3): 775-793. doi:10.5194/tc-2018-141

558 Frantz, C. M. and Light, B., et al., 2019. Physical and optical characteristics of heavily melted "rotten"
559 Arctic sea ice. The Cryosphere, 13 (3): 775-793. doi:10.5194/tc-13-775-2019

560 Grenfell, T. C., 1983. A theoretical model of the optical properties of sea ice in the visible and near
561 infrared. Journal of Geophysical Research: Oceans, 88 (C14): 9723-9735.
562 doi:10.1029/JC088iC14p09723

563 Grenfell, T. C., 1991. A radiative transfer model for sea ice with vertical structure variations. Journal of
564 Geophysical Research: Oceans, 96 (C9): 16991-17001. doi:10.1029/91JC01595

565 Grenfell, T. C. and Light, B., et al., 2006. Spectral transmission and implications for the partitioning of
566 shortwave radiation in arctic sea ice. Annals of glaciology, 44 (1): 1-6.
567 doi:10.3189/172756406781811763

568 Grenfell, T. C. and Perovich, D. K., 1981. Radiation Absorption Coefficients of Polycrystalline ice from
569 400 to 1400 nm. Journal of Geophysical Research, 86 (C8): 7447-7450.
570 doi:10.1029/2007JD009744

571 Grenfell, T. C. and Perovich, D. K., 2008. Incident spectral irradiance in the Arctic Basin during the
572 summer and fall. Journal of Geophysical Research, 113: D12117. doi:10.1029/2007JD009418

573 Grenfell, T. C. and Warren, S. G., 1999. Representation of a nonspherical ice particle by a collection of
574 independent spheres for scattering and absorption of radiation. Journal of Geophysical Research,
575 104 (D24): 31697-31709. doi:10.1029/1999JD900496

576 Hamre, B., 2004. Modeled and measured optical transmittance of snow-covered first-year sea ice in
577 Kongsfjorden, Svalbard. Journal of Geophysical Research, 109 (C10).
578 doi:10.1029/2003JC001926

579 Hansen, J. E. and Travis, L. D., 1974. Light scattering in planetary atmosphere. Space Science Reviews,
580 16: 527-610. doi:10.1007/BF00168069

581 Hunke, E. C. and Notz, D., et al., 2011. The multiphase physics of sea ice: a review for model developers.
582 The Cryosphere, 5 (4): 989-1009. doi:10.5194/tc-5-989-2011

583 Katlein, C. and Arndt, S., et al., 2015. Influence of ice thickness and surface properties on light
584 transmission through Arctic sea ice. Journal of Geophysical Research: Oceans, 120 (9): 5932-
585 5944. doi:10.1002/2015JC010914

586 Katlein, C. and Arndt, S., et al., 2019. Seasonal Evolution of Light Transmission Distributions Through

587 Arctic Sea Ice. *Journal of Geophysical Research: Oceans*, 124 (8): 5418-5435.
588 doi:10.1029/2018JC014833

589 Kattlein, C. and Valcic, L., et al., 2021. New insights into radiative transfer within sea ice derived from
590 autonomous optical propagation measurements. *The Cryosphere*, 15 (1): 183-198. doi:10.5194/tc-
591 15-183-2021

592 Kwok, R., 2018. Arctic sea ice thickness, volume, and multiyear ice coverage: losses and coupled
593 variability (1958-2018). *Environmental research letters*, 13 (10): 105005. doi:10.1088/1748-
594 9326/aae3ec

595 Kwok, R. and Cunningham, G. F., 2016. Contributions of growth and deformation to monthly variability
596 in sea ice thickness north of the coasts of Greenland and the Canadian Arctic Archipelago.
597 *Geophysical Research Letters*, 43 (15): 8097-8105. doi:10.1002/2016GL069333

598 Landy, J. C. and Ehn, J. K., et al., 2015. Albedo feedback enhanced by smoother Arctic sea ice.
599 *Geophysical Research Letters*, 42 (24): 10,714-10,720. doi:10.1002/2015GL066712

600 Lei, R. and Tian-Kunze, X., et al., 2016. Changes in summer sea ice, albedo, and portioning of surface
601 solar radiation in the Pacific sector of Arctic Ocean during 1982-2009. *Journal of Geophysical
602 Research: Oceans*, 121 (8): 5470-5486. doi:10.1002/2016JC011831

603 Light, B. and Grenfell, T. C., et al., 2008. Transmission and absorption of solar radiation by Arctic sea
604 ice during the melt season. *Journal of Geophysical Research*, 113: C03023.
605 doi:10.1029/2006JC003977

606 Light, B. and Maykut, G. A., et al., 2003. Effects of temperature on the microstructure of first-year Arctic
607 sea ice. *Journal of Geophysical Research: Oceans*, 108 (C2): 3051. doi:10.1029/2001JC000887

608 Light, B. and Maykut, G. A., et al., 2004. A temperature-dependent, structural-optical model of first-year
609 sea ice. *Journal of Geophysical Research*, 109: C06013. doi:10.1029/2003JC002164

610 Light, B. and Perovich, D. K., et al., 2015. Optical properties of melting first - year Arctic sea ice. *Journal
611 of Geophysical Research: Oceans*, 120 (11): 7657-7675. doi:10.1002/2015JC011163

612 Light, B. and Smith, M. M., et al., 2022. Arctic sea ice albedo: Spectral composition, spatial heterogeneity,
613 and temporal evolution observed during the MOSAiC drift. *Elementa: Science of the
614 Anthropocene*, 10 (1). doi:10.1525/elementa.2021.000103

615 Lindsay, R. and Schweiger, A., 2015. Arctic sea ice thickness loss determined using subsurface, aircraft,
616 and satellite observations. *The Cryosphere*, 9 (1): 269-283. doi:10.5194/tc-9-269-2015

617 Macfarlane, A. R. and Dadic, R., et al., 2023. Evolution of the microstructure and reflectance of the
618 surface scattering layer on melting, level Arctic sea ice. *Elementa: Science of the Anthropocene*,
619 11 (1). doi:10.1525/elementa.2022.00103

620 Markus, T. and Stroeve, J. C., et al., 2009. Recent changes in Arctic sea ice melt onset, freezeup, and melt
621 season length. *Journal of Geophysical Research*, 114: C12024. doi:10.1029/2009JC005436

622 Mobley, C. D. and Cota, G. F., et al., 1998. Modeling Light Propagation in Sea Ice. *IEEE Transactions
623 on Geoscience and Remote Sensing*, 36 (5): 1743-1749. doi:10.1109/36.718642

624 Mortin, J. and Svensson, G., et al., 2016. Melt onset over Arctic sea ice controlled by atmospheric
625 moisture transport. *Geophysical Research Letters*, 43 (12): 6636-6642.
626 doi:10.1002/2016GL069330

627 Nicolaus, M. and Hoppmann, M., et al., 2021. Snow depth and air temperature seasonality on sea ice
628 derived from snow buoy measurements. *Frontiers in Marine Science*, 8.
629 doi:10.3389/fmars.2021.655446

630 Notz, D. and Worster, M. G., 2009. Desalination processes of sea ice revisited. *Journal of Geophysical
631 Research*, 114 (C5). doi:10.1029/2008JC004885

632 Parkinson, C. L. and Comiso, J. C., 2013. On the 2012 record low Arctic sea ice cover: Combined impact
633 of preconditioning and an August storm. *Geophysical Research Letters*, 40 (7): 1356-1361.
634 doi:10.1002/grl.50349

635 Perovich, D. K., 2003. Complex yet translucent: the optical properties of sea ice. *Physica B: Condensed
636 Matter*, 338 (1-4): 107-114. doi:10.1016/S0921-4526(03)00470-8

637 Perovich, D. K., 2003. Thin and thinner: Sea ice mass balance measurements during SHEBA. *Journal of
638 Geophysical Research*, 108 (C3). doi:10.1029/2001JC001079

639 Perovich, D. and Light, B., et al., 2020. Changing ice and changing light: trends in solar heat input to the
640 upper Arctic ocean from 1988 to 2014. *Annals of Glaciology*, 61 (83): 401-407.
641 doi:10.1017/aog.2020.62

642 Perron, C. and Kattlein, C., et al., 2021. Development of a diffuse reflectance probe for in situ
643 measurement of inherent optical properties in sea ice. *The Cryosphere*, 15 (9): 4483-4500.
644 doi:10.5194/tc-15-4483-2021

645 Persson, P. O. G., 2012. Onset and end of the summer melt season over sea ice: thermal structure and
646 surface energy perspective from SHEBA. *Climate Dynamics*, 39 (6): 1349-1371.
647 doi:10.1007/s00382-011-1196-9

648 Petrich, C. and Eicken, H., 2010. Growth, Structure and Properties of Sea Ice in Thomas, DN,
649 Dieckmann, GS eds., *Sea ice*. 2nd ed. Hoboken, NJ: Wiley Online Library.

650 Petty, A. A. and Stroeve, J. C., et al., 2018. The Arctic sea ice cover of 2016: a year of record-low highs
651 and higher-than-expected lows. *The Cryosphere*, 12 (2): 433-452. doi:10.5194/tc-12-433-2018

652 Ricker, R. and Hendricks, S., et al., 2017. A weekly Arctic sea-ice thickness data record from merged
653 CryoSat-2 and SMOS satellite data. *The Cryosphere*, 11 (4): 1607-1623. doi:10.5194/tc-11-1607-
654 2017

655 Rigor, I. G. and Wallace, J. M., 2004. Variations in the age of Arctic sea-ice and summer sea-ice extent.
656 *Geophysical Research Letters*, 31 (9): n/a-n/a. doi:10.1029/2004GL019492

657 Smedley, A. R. D. and Evatt, G. W., et al., 2020. Solar radiative transfer in Antarctic blue ice: spectral
658 considerations, subsurface enhancement, inclusions, and meteorites. *The Cryosphere*, 14 (3): 789-
659 809. doi:10.5194/tc-14-789-2020

660 Smith, M. M. and Light, B., et al., 2022. Sensitivity of the Arctic Sea Ice Cover to the Summer Surface
661 Scattering Layer. *Geophysical Research Letters*, 49 (9): e2022GL098349.
662 doi:10.1029/2022GL098349

663 Smith, R. C. and Baker, K. S., 1981. Optical properties of the clearest natural waters (200 - 800 nm).
664 *Applied Optics*, 20 (2): 177. doi:10.1364/AO.20.000177

665 Stroeve, J. and Notz, D., 2018. Changing state of Arctic sea ice across all seasons. *Environmental research
666 letters*, 13 (10): 103001. doi:10.1088/1748-9326/aade56

667 Timmermans, M. L., 2015. The impact of stored solar heat on Arctic sea ice growth. *Geophysical
668 Research Letters*, 42 (15): 6399-6406. doi:10.1002/2015GL064541

669 Tschudi, M. A. and Meier, W. N., et al., 2020. An enhancement to sea ice motion and age products at the
670 National Snow and Ice Data Center (NSIDC). *The Cryosphere*, 14 (5): 1519-1536. doi:10.5194/tc-
671 14-1519-2020

672 Tschudi, M. and Meier, W., et al., 2019. EASE-Grid Sea Ice Age, Version 4. [Indicate subset used].
673 Boulder, Colorado USA. NASA National Snow and Ice Data Center Distributed Active Archive
674 Center.. doi:10.5067/UTAV7490FEPB

675 Tucker, W. B. and Perovich, D. K., et al., 1992. Physical Properties of Sea Ice Relevant to Remote Sensing.
676 *Microwave Remote Sensing of Sea Ice*, American Geophysical Union: 9-28.

677 Vancoppenolle, M. and Fichefet, T., et al., 2009. Simulating the mass balance and salinity of Arctic and
678 Antarctic sea ice. 2. Importance of sea ice salinity variations. *Ocean Modelling*, 27 (1-2): 54-69.
679 doi:10.1016/j.ocemod.2008.11.003

680 Veyssi  re, G. and Castellani, G., et al., 2022. Under-Ice Light Field in the Western Arctic Ocean During
681 Late Summer. *Frontiers in Earth Science*, 9. doi:10.3389/feart.2021.643737

682 Wang, Q. and Lu, P., et al., 2020. Physical Properties of Summer Sea Ice in the Pacific Sector of the
683 Arctic During 2008 - 2018. *Journal of Geophysical Research: Oceans*, 125 (9).
684 doi:10.1029/2020JC016371

685 Weeks, W. F. and Ackley, S. F., 1986. The Growth, Structure, and Properties of Sea Ice.

686 Yu, M. and Lu, P., et al., 2022. Impact of Microstructure on Solar Radiation Transfer Within Sea Ice
687 During Summer in the Arctic: A Model Sensitivity Study. *Frontiers in marine science*, 9 (861994).
688 doi:10.3389/fmars.2022.861994

689 Zhang, J. and Schweiger, A., et al., 2018. Melt Pond Conditions on Declining Arctic Sea Ice Over 1979 -
690 2016: Model Development, Validation, and Results. *Journal of Geophysical Research: Oceans*,
691 123 (11): 7983-8003. doi:10.1029/2018JC014298

692